Original Study **Open Access**

Bruno Giovanni*, Guerra Laura

DEM modelling of the activation and reactivation of capable faults in a typical Apulian rock succession: the viewpoint of local seismic effect during the 1948 Earthquake (Apulia, Italy)

https://doi.org/10.2478/sgem-2025-0001
received October 10, 2023; accepted December 16, 2024.

Abstract: The extension and magnitude of deformations induced by the fault ruptures, especially in active and capable faults, have a significant impact on the integrity of anthropogenic surface structures and the way water and pollutants migrate underground. The purposes of this study are twofold. The first is to delineate the rupture mechanisms, the location and extent of the damage zone associated with the type of fault considered. The second is to assess the magnitude of coseismic displacements and local seismic response (LSR), in the case of surface propagation of a pre-existing active and capable normal fault. In previous studies, the lithotypes modelled had homogeneous and isotropic geotechnical behaviour unlike the lithoid and anisotropic lithotypes used in the present study. In addition, they used a generic time history of accelerations for the dynamic analyses that are non-seismocompatible to the expected seismicity in the case study geological–structural context.

Numerical modelling of fault ruptures propagation through a typical stratigraphic series of an Apulian geostructural setting was performed using the distinct element method (DEM) code UDEC. In the dynamic analysis, the seismic input applied to the bottom of the calcareous bedrock was based on relevant seismological theories and on the historical seismicity of the current 'Candelaro' fault area case study. Given the significant congruity between the results of the previous studies and those obtained in the quasi-static parametric analyses and in the dynamic local seismic response (LSR) ones, it is shown that the validity of the strength criteria and physical–mechanical parameters used in the modelling can be confirmed. Increasing use of this approach for the study of faults, capable and not, could allow the creation of a conspicuous database on a regional level, which aims to a better land planning and reduction of its seismic and hydrogeological vulnerability.

Keywords: active and capable faults; distinct element numerical analysis; Local Seismic Response (LSR); seismic vulnerability; hydrogeological vulnerability.

1 Introduction

A wide portion of the Italian territory is at high seismic risk because of both the high number of earthquakes recorded and the magnitude of some of them. This risk is due to several factors such as high population density in some areas, heterogeneity in building types, and presence of historic-monumental buildings. However, the main factor remains the basic seismic hazard of the territory. The majority of earthquakes recorded in Italy are of tectonic nature; however, some earthquakes of volcanic origin are localised in specific areas of the territory and generally of low magnitude. This means that these earthquakes are caused by the formation and/or reactivation of fault ruptures as a result of intra- and inter-plate movements.

Even the Apulian region, with its role as the foreland of the Apennine orogen to the west and the Dinaric-Ellenic orogen to the east, is not exempt from earthquakes. Seismic events are often from seismogenic zones east of the Adriatic Sea and sometimes, as in the case study discussed here, generated in seismogenic areas of active and capable faults that fall within the Apulian foreland.

Fault ruptures generate seismic waves and cause a zone of deformation called the *fault zone* in the rocks that host them. In the case of capable faults, these deformations propagate up to the ground surface, generating damage to buildings and infrastructures, in addition to those

***Corresponding author: Bruno Giovanni,** Politecnico di Bari, Department of Civil, Environmental, Land, Building Engineering and Chemistry, via Orabona 4, 70125 Bari, Italy, E-mail: giovanni.bruno@poliba.it
Guerra Laura, Free lance geologist, viale Divisione Julia 71, 36100 Vicenza, Italy

Open Access. © 2025 Bruno Giovanni, Guerra Laura, published by Sciendo. This work is licensed under the Creative Commons Attribution alone 4.0 License.

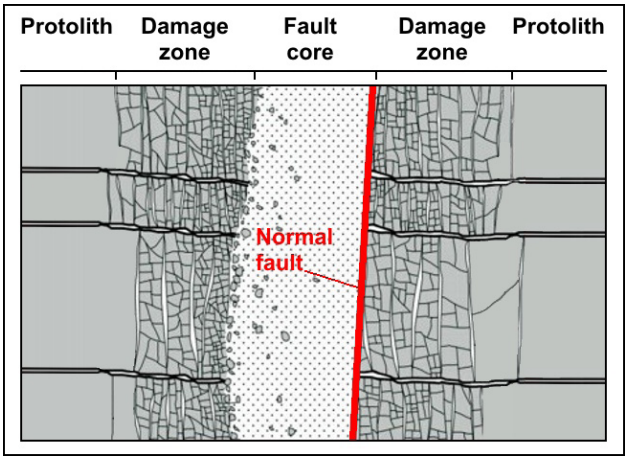

Figure 1: Constitutive elements of a *fault zone* (from: [10] modified).

generated by the vibrations produced by seismic waves. The rock volume of the *fault zone* can be schematised into the following three portions, each characterised by lithological, structural and hydrogeological peculiarities: the *fault core*, the *damage zone* and the *undeformed bedrock* or *protolith* (Fig. 1).

The extent and magnitude of brittle and plastic deformations induced by fault rupture propagation (damage zone) have a significant impact on the permeability of the rock mass. This generally results in increased permeability and vulnerability to the transport of pollutants released to the surface, especially in the case of karst underground aquifers [8], [9], [10], [30], [47]. Of utmost importance are the effects of LSR that occur in inactive faults and, above all, during the activation/reactivation of active and capable faults [53], [57], [44] on the integrity of anthropic surface structures [29] and on the coseismic effects that can be generated (landslides, subsidence, displacements, etc.).

In previous studies [44], [45], [46], [49], [50], the lithotypes modelled had homogeneous and isotropic geotechnical behaviour unlike the lithoid and anisotropic lithotypes used in the present study. Furthermore, a generic time history of accelerations was used for the dynamic analyses, which is not compatible with the expected seismicity in the geological–structural context of the case study, as required by the building regulations (NTC18) in Italy [52]. Finally, no LSR assessment was carried out on the ground surface involved in the fault damage zone. The use of appropriate numerical codes and properly parameterised geomechanical models is indispensable in understanding the mechanisms governing such phenomena as well as in defining their magnitude and areal extension. Therefore, in order to overcome the limitations posed by previous studies, it was decided to carry out DEM numerical simulations of the deformation and LSR phenomena associated with the formation or reactivation of a capable fault in a stratigraphic sequence consisting of competent and anisotropic rock masses such as those typical of the Apulian area.

2 Geostructural setting of the ‘Candelaro’ fault area (west edge of Gargano promontory)

The structural setting of the case study area [60], [61] is characterised by the presence of a fault system, the most famous of which is known in the literature as the ‘Candelaro’ fault, which forms the dividing boundary between two geodynamic domains, the foreland domain to the east, consisting of the Gargano promontory, and the Bradanica foredeep domain to the west, consisting of the ‘Tavoliere delle Puglie’ plain. The system consists of several NW–SE-oriented faults that have undergone polyphase tectonics during the Mesozoic to Quaternary period [24], and currently, they exhibit a kinematism of right trans-tensional fault with a predominantly normal component [58], [63]. Of these faults, the one considered for the case study (pink in Fig. 2) consists of two stretches, displaced by the extensive W–E transcurrent, right-handed shear system of the ‘San Marco in Lamis-Mattinata’ fault.

Lithostratigraphically, the foreland domain in this area consists of an approximately 350-m thick bedrock of carbonate platform rocks referable to the Jurassic-Cretaceous [27], [60]. It consists of light grey and light brown limestones and dolomites in 0.30- to 2-m thick layers plunging southeastward at a 10–20° dip. In transgression on the bedrock are Plio-Pleistocene calcarenites, which are about 40-m thick and are known in the literature as ‘Gravina limestones’ [60]. These are yellow-ochre biocalcarenites with variable degree of cementation and massive appearance. In the foredeep domain of the Apulian Tavoliere Plain, above the Gravina Calcarenites there are sub-Apennine Clays of the Pliocene sup.- Pleistocene inf. which are followed by marine and continental regressive deposits of the Pleistocene that constitute different orders of terraces.

The stratigraphic succession consisting of a bedrock of faulted Mesozoic limestones covered by Gravina calcarenites is typical not only of the case study area but of the whole Apulian foreland. For this reason, it was chosen as representative to implement parametric numerical modelling and simulation of the local seismic response in the case study of reactivation of the ‘Candelaro’ fault.

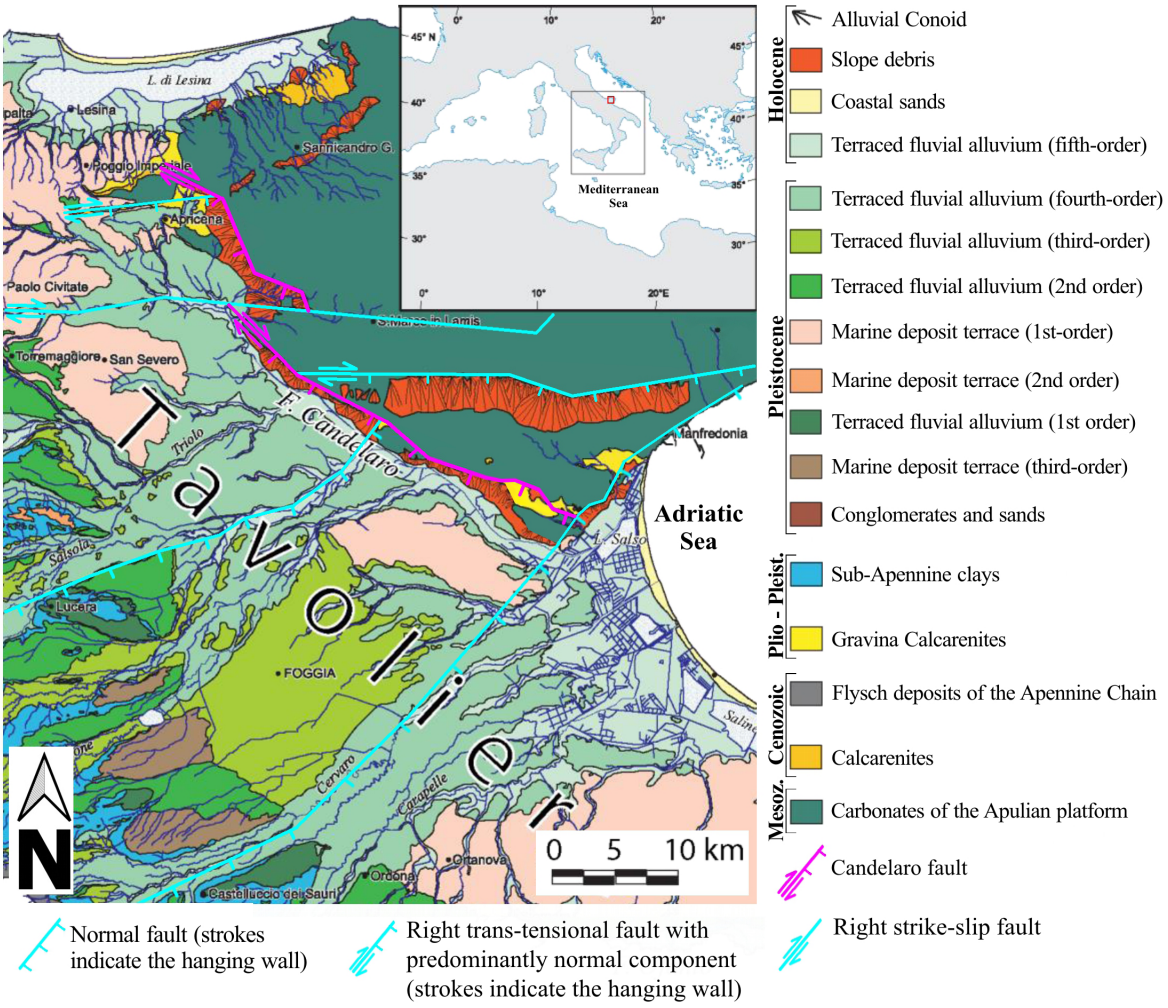

Figure 2: Schematic geostructural map of the 'Candelaro' fault area (from: [27] modified).

3 Methodology

Previous studies on the propagation of fault plane rupture have been conducted with numerical simulations [4], [44], [46], [49], [51], [62]; physical model tests [11], [20], [43], [44], [50]; and *in situ* meso- and micro-structural geology surveys [12], [21], [22], [29], [42], [47]. Particularly, numerical simulations were essentially parametric in nature and focused on different types of faulting, certain lithotypes, such as sands and clays and the effects of earthquake ground motion [12], [13], [45]. The lithotypes modelled in previous studies, however, had homogeneous and isotropic geotechnical behaviour unlike the lithoid and anisotropic lithotypes used in the present study. In addition, a generic time history of accelerations was used for the dynamic analyses, in agreement with the displacements expected by [87], but unrelated to the expected seismicity in a real geological–structural context.

The methodology and numerical code used in this paper have made it possible to expand the field of knowledge on the mechanisms of coseismic rupture, in the case of reactivation of an active and capable normal fault and on the LSR in the projection area of the fault plane onto the ground level. The analytical process is divided into two parts, as described below.

4 Seismic characterisation of the 'Candelaro' fault and selection of the input motion

The case study fault area is affected by intense seismic activity both historically and instrumentally (Fig. 3). In particular, the seismic sequence of August 18–22, 1948, with quakes on August 18th (21:12 GMT), 21st (08:45

Figure 3: Seismicity of the 'Candelaro' fault area: a) historical and instrumental seismicity (from: [33, 34] modified) and b) depth and magnitude of earthquakes (from: [39] modified).

GMT) and 22nd (23:16 GMT) and epicentre located on the 'Candelaro' fault, recorded a macroseismic intensity (MCS) I_{max}= 6.5–7 and moment magnitude M_w= 5.3–5.5 [33], [34]. This fault in accordance with commonly accepted definitions in literature studies [36], [37] is to be classified as active and capable. As a matter of fact, it was definitely active until the upper Pleistocene [40] and it is capable of being reactivated by the right shear system of the composite seismogenic sources ITCS058 – San Marco in Lamis-Mattinata and ITCS003 – Ripabottoni–San Severo, which divide it into two trunks [28]. Evidence that the 'Candelaro' fault is capable of creating ruptures on the topographic surface is the seismic sequence of the year 1948 that caused extensive damage and opened a 12-cm wide, 50-cm long and about 3-m deep fissure in the ground in 'contrada Ripa' of the town of Rignano Garganico from which gas escaped [55].

Observational data from field studies and theoretical studies suggest that an earthquake magnitude (M_w) can correlate with the seismic moment (M_o) and the amount of displacement (D) along the causative fault by means of the following equation [35]

$$D=M_o/(G_i*RA) \quad (1)$$

where: G_i= (GPa) rock shear modulus; $RA = 10^{[-2.87+(0.82*M_w)]}$ (km^2); area of a normal fault surface ruptured [64]; $M_o=10^{[3/2\ (5.7+M_w)]}$ seismic moment [35]

The aforementioned equation proposed by Hanks and Kanamori [35] was implemented using values of the shear modulus G_i = 25GPa, already used for the case study rock in previous numerical modelling [14], [16], [18], [35] and usually assumed for crustal faults in the literature [64], [65], and a moment magnitude M_w = 5.5 that characterises the seismicity of the 'Candelaro' fault case study [33], [34]. Consequently, it was possible to estimate that in the case of a remobilisation of the 'Candelaro' fault by an earthquake of magnitude M_w = 5.5, the value of the average displacement expected along the fault plane would be D = 0.92 m. This value is a useful reference for evaluating the accuracy of the results of the numerical analysis of LSR.

The accelerograms used for the dynamic and LSR of the case study analysis were obtained with REXEL software [38] from the European Strong-motion Database [2], [3]. Consultation of the database was done using the search parameters given in Table 1 and respecting the seismo-compatibility criteria according to the current Italian seismic building code (NTC18) [52].

The average spectra of horizontal and vertical accelerations of seismic motion, used as an input for the dynamic and LSR analyses, were plotted together with the elastic spectra for rigid substrate of cat. 'A' and horizontal topography according to the current Italian seismic regulations (Fig. 4).

5 DEM numerical quasi-static and dynamic-LSR simulations

Numerical simulations were conducted on a geomechanical model consisting of a rigid layered bedrock and a weak, massive, calcarenitic cover (Fig. 5). This stratigraphic succession is typical of the Apulian foreland

Table 1: Input parameters for searching accelerograms in the seismological European Strong-motion database.

Acceleration component	Magnitude range	Epicentral distance range (km)	Site class	Topographic class	Nominal life (years)	Usage class	Limit state	Scaled records
Horizontal	5.6–7	0–20	A	T_1	50	II	SLV	No
Vertical	5.2–7	0–30	A	T_1	50	II	SLV	Yes

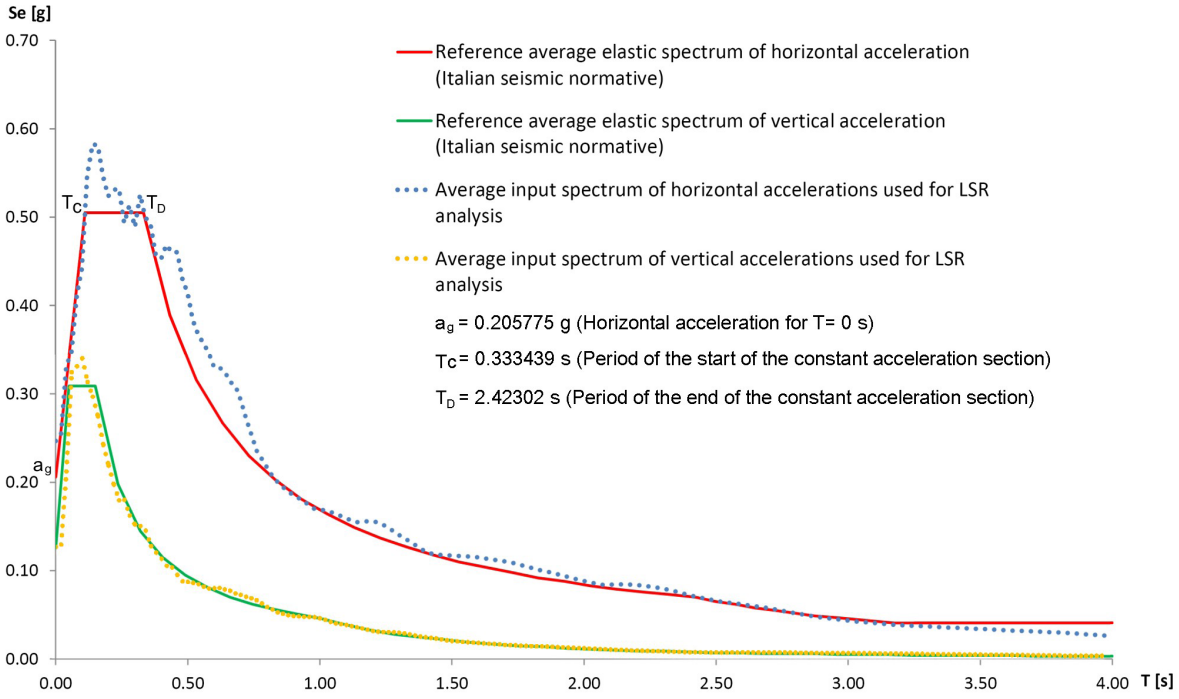

Figure 4: Average input spectra of horizontal and vertical accelerations used for LSR analysis, compared with elastic spectra for rigid substrate of cat. 'A' and horizontal topography [52].

where the attitude and thickness of the bedrock limestone layers (s = 0.80–1.0 m) were inferred from previous *in-situ* surveys in the case study area [38] and has already been described in Section 2. The 500-m length of the model was chosen in accordance with the requirements of current Italian and international technical standards on seismic microzonation [25], [48] regarding the extent of the area of attention straddling an active and capable fault. The thickness of the calcarenitic cover was chosen in accordance with what the lithotype presents in the case study area. A value of 100 m was set for the limestone bedrock sufficient for the faulting process to be fully developed in the model.

The simulations performed concerned the rupture propagation mechanisms of normal and inverse faults through the bedrock to the ground surface in quasi-static parametric analyses. Moreover, a dynamic analysis with local seismic response LSR evaluation was carried out for the case study of the 'Candelaro' normal fault.

According to previous studies [20], [44], [45], [46], [53], [57] in the quasi-static parametric analyses, velocity vectors oriented to generate shear rupture along normal and reverse fault planes, dip at 30°, 45° and 60°, were applied to the edges of the left portion of the undisturbed geomechanical models (black arrows in Fig. 6 a). This first phase of the simulations was preparatory to provide the model used for the dynamic LSR analysis, which focused on the propagation of the fault rupture, under the assumption of seismic reactivation of the normal fault plane in the considered case study. Moreover, the parametric analysis aimed to delineate the trend and magnitude of brittle and plastic deformations along a fault plane that generates and propagates in a succession of lithoid rocks with different elasto-plastic behaviour, as

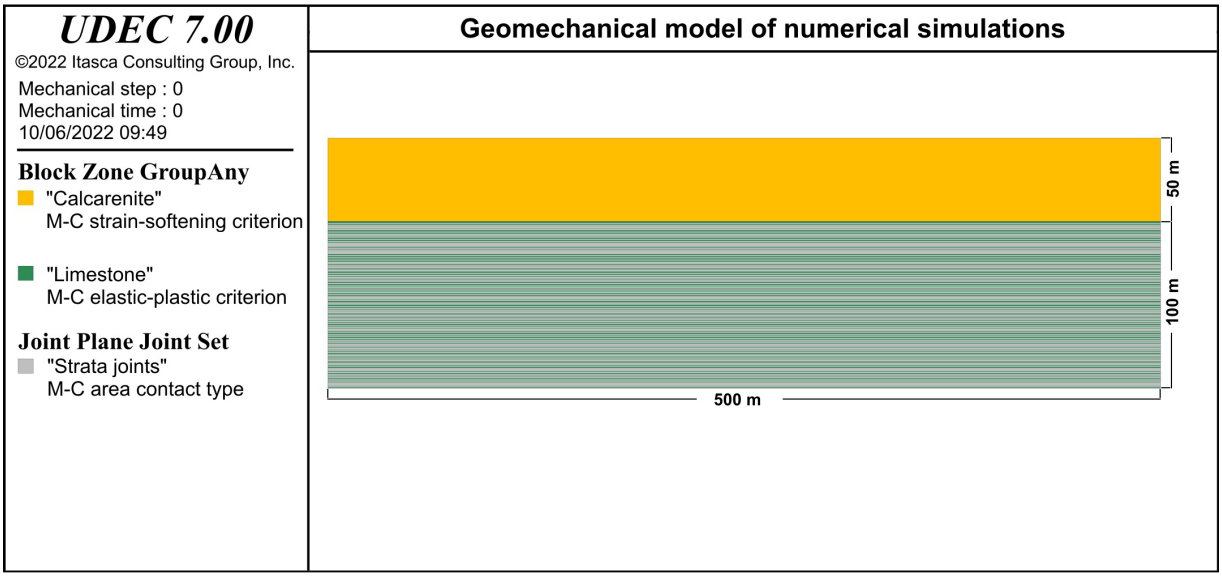

Figure 5: Geomechanical model used for numerical simulations.

the kinematism (normal and reverse faults) and the dip angles of the faults change.

The boundary conditions of the model in Fig. 6a consist of a velocity magnitude of 0.01 m/s (to minimise inertial effects) applied to the several quasi-static analyses. All quasi-static simulations were conducted for a sufficient number of computational steps to create a fault plane with displacements of about 1–3 m in the models. This is consistent with the maximum displacement values estimated to be generated in the case study considered during a single seismic event in literature studies [35], [64] and with the extent of fractures observed in situ after the 1948 summer seismic sequence in the case study of the 'Candelaro' fault [34], [55].

5.1 Geomechanical characterisation of the modelled sections

Physical–mechanical parameterisation of the lithotypes in the geomechanical model was done using literature data and previously used numerical simulations with the UDEC code [16], [18], [19]. According to the extensive literature on the Plio-Pleistocene calcarenites outcropping in Apulia, the physical–mechanical characteristics (Table 2) are highly variable depending on limestone cement content, grain size assortment and degree of saturation [5], [15], [17], [23], [26], [59].

In particular, the uniaxial compressive strength value of these calcarenites allows them to be classified as a soft rock [31]. Moreover, due to their strain-softening behaviour, the friction angle, cohesion, tensile strength and dilation angle have been reduced linearly from its peak values to their residual values during a development of 3% plastic strain [19].

Reference was made to data published in literature studies [14], [16], [18] also regarding the physical–mechanical parameters of the Mesozoic limestones, their layer discontinuities and faults (Table 3).

5.2 Mesh configuration and boundary conditions of the analyses

The analyses were conducted considering deformable blocks, using the code UDEC v.7.00_78 [41], adopting the Mohr–Coulomb strength criterion and strain-softening constitutive models for the calcarenitic lithotype and linear elastic-plastic models for the layered limestone lithotype, respectively. For the fault planes and layer discontinuities of the limestone rock mass, the Mohr–Coulomb criterion and the 'area contact' type were adopted. Simulations were performed in terms of effective stress and dry conditions by means of sections with a width–height ratio of 5:1, which is enough to minimise the effects of lateral boundaries on the strain development in the model. To avoid numerical distortion of the propagating wave in the dynamic-LSR analysis, the maximum length of the grid elements should be assumed smaller than 1/10 of the wavelength λ_{min} associated with the highest frequency of the used seismic input motion. For this purpose, all the modelled sections have been meshed via a 5-m maximum

Table 2: Minimum, maximum and residual values of calcarenite physical–mechanical parameters (from: [5], [15], [17], [23], [26], [59]).

Physical–mechanical parameters for Mohr–Coulomb Strain-Softening criterion											
Lithotype	**Natural unit weight γ_a (kN/m³)**	**Porosity n_{min} - n_{max} (%)**	**Imbibition coefficient Ci_{min} - Ci_{max} (%)**	**Friction angle φ_{res} - φ_{max} (degrees)**	**Cohesion c_{res} - c_{max} (MPa)**	**UCS strength σ_{cmax} (MPa)**	**Tensile strength σ_{tres} - σ_{tmax} (MPa)**	**Young modulus E_{max} (GPa)**	**Bulk modulus K_{max} (GPa)**	**Shear modulus G_{max} (GPa)**	**Dilation angle Δ_{res} - Δ_{max} (degrees)**
Gravina Calcarenite	19	35 - 50	15 - 40	30 - 38	0.13 - 0.29	2.0	0.11 - 0.26	3.5	2.9	1.3	3 - 5

Table 3: Values of physical–mechanical parameters of limestone, layer discontinuities and faults (from: [14], [16], [18]).

Physical–mechanical parameters for Mohr–Coulomb elasto-plastic criterion									
Lithotype	**Natural unit weight γ_a (kN/m³)**	**Friction angle φ_i (degrees)**	**Cohesion c_i (MPa)**	**UCS strength σ_{ci} (MPa)**	**Tensile strength σ_{ti} (MPa)**	**Young modulus E_i (GPa)**	**Bulk modulus K_i (GPa)**	**Shear modulus G_i (GPa)**	**Dilation angle (degrees)**
Altamura Limestone	24	50	13	69	11	60	33	25	7
Mechanical parameters of discontinuities for Mohr–Coulomb 'area-contact' criterion									
Rock mass	Joint type	Joint normal stiffness JKN (GPa/m)	Joint shear stiffness JKS (GPa/m)	Joint tensile strength J_{tens} (MPa)	Joint friction angle J_{fric} (degrees)	Joint cohesion J_{coh} (MPa)	Layers dip (degrees)	Layers spacing (m)	Joint dilation angle (degrees)
Altamura Limestone	Layers and faults	249	104	0.70	39	5.29	0	0.80	7

length, triangular finite difference grid elements. In the quasi-static analyses (Fig. 6a), a constant velocity oriented as the dip angle of the simulated fault was applied to the mesh boundary of the left portion of the undeformed geomechanical model. At the right portion of the model, on the other hand, zero velocities were imposed in the X- and Y-directions.

The number of calculation steps applied was the same for all parametric simulations. In addition, the velocity increments were in the order of 0.01 m/s, to minimise inertial effects and have quasi-static analyses.

For the simulation of the coseismic ruptures and LSR due to the specific presence and reactivation of the case study fault, two distinct models obtained from the static analyses were used where displacements and velocities were set to zero and only the plasticisation states of the rocks were maintained. The first model (Fig. 6b) has no fault plane; the second, more realistic model has a pre-existing normal fault plane with a 45° dip (Fig. 6c). Supplementary free-field grids coupled to viscous boundaries have been used, to prevent reflection of outward propagating waves back into the numerical model. These consisted in independent dashpots in the normal and shear direction [41]. A 59.99 second seismic waves input was applied at the bottom of limestone bedrock with an incidence angle $\theta = 0°$, and the time histories of velocity associated to the corresponding acceleration records were converted into shear and normal stress time histories (Fig. 7), as usual when using quiet boundaries. Furthermore, a viscous Rayleigh damping with $\xi_{min} = 3\%$ and a frequency $f_{min} = 16$ Hz were used.

6 Results and discussion

6.1 Quasi-static parametric analyses

The quasi-static parametric analyses have been conducted on a typical Apulian stratigraphic succession (Fig. 8) by

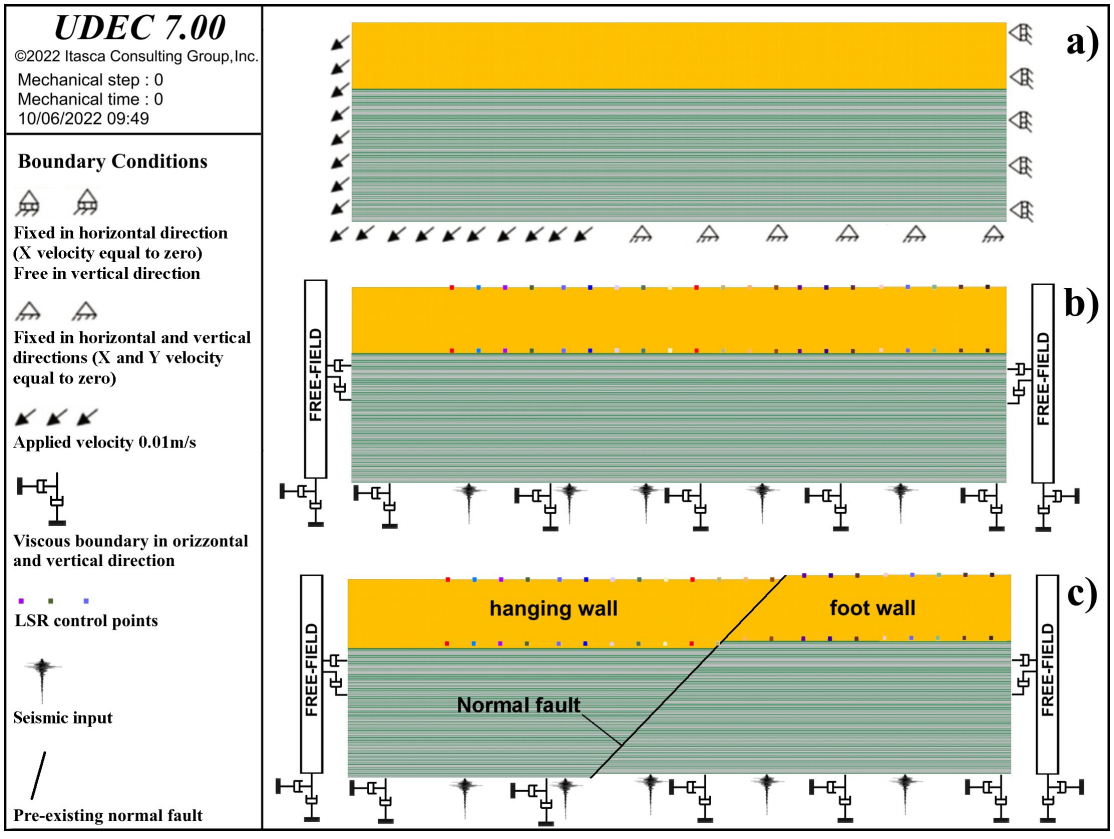

Figure 6: Models and boundary conditions used in the numerical analyses: a) quasi-static; b) dynamic and LSR (model without pre-existing fault); c) dynamic and LRS (case study with reactivation of a pre-existing normal fault plane 45° dip).

varying the kinematism (normal and reverse faults) and the dip angles of the faults (Table 4).

The results obtained, in terms of type of failure, displacements and fault core and damage zone extents on the ground level, are in fair agreement with those of previous studies [44], [45], [46], [53]. However, it must be pointed out that more of these previous studies were not conducted with a distinct element code but with finite difference codes (FLAC) or finite element codes (ABAQUS) and using models that do not include the layered and faulted substrate in addition to the cover soil (Fig. 6). The distinct-element UDEC code, on the other hand, is well suited for modelling the growth of discontinuities or cover soil deformations under large strains [1], [20], [62]. In addition, this technique can model deformations involving unlimited relative motions of individual elements like strata and rock blocks. In the fault core zone, the propagation of displacements, from the bedrock to the ground level through the calcarenitic cover, deviates slightly from the straight projection of the bedrock fault plane. This phenomenon is most evident in cases of reverse faults, where the damage zone in the calcarenitic cover tends to be more extensive and has a lower dip than the fault plane in the substrate. In all simulations, regardless of the kinematics (normal or reverse) and the dip angles of the faults, the maximum displacements were obtained in the fault hanging wall of the calcarenitic cover (Fig. 8). As for the brittle and plastic failure mechanisms of the rock mass of the limestone substrate and calcarenitic cover, it is observed that they are caused by shear and, subordinately, tensile stresses. In the case of normal faults, the main shear plane tends to split into two conjugate planes as it transfers from the calcarenitic cover to the substrate. This phenomenon is more evident for fault planes that dip at 60° (Fig. 8f, left).

In cases of reverse faults that dip at 30° and 45°, imbricated fan shear structures are generated from the separation boundary between the limestone substrate and the calcarenitic cover and up to the surface of the models (Figs. 8b, d, right). Several conjugate fracture shear planes are also generated, especially in the case of a reverse fault dip at 60° (Fig. 8f, right), which affect the fault footwall of the calcarenitic cover.

Table 4: Quasi-static analyses: failure types, maximum displacement values, extents of fault core and damage zone.

Kinematism	Dip angles (degrees)	Type of failure	Maximum displacement on the ground level (m)	Extent of fault core zone on the ground level (m)	Extent of the damage zone on the ground level (m)
Normal fault	30	Conjugate failure surfaces	1.49	6.50	9.90
	45	Single failure surface	1.83	7.70	9.60
	60	Conjugate failure surfaces	2.58	7.80	9.50
Reverse fault	30	Trailing imbricate fan and conjugate surfaces	1.48	26.50	84.50
	45	Trailing imbricate fan and conjugate surfaces	1.82	56.10	61.50
	60	Conjugate failure surfaces	2.57	20.70	163.20

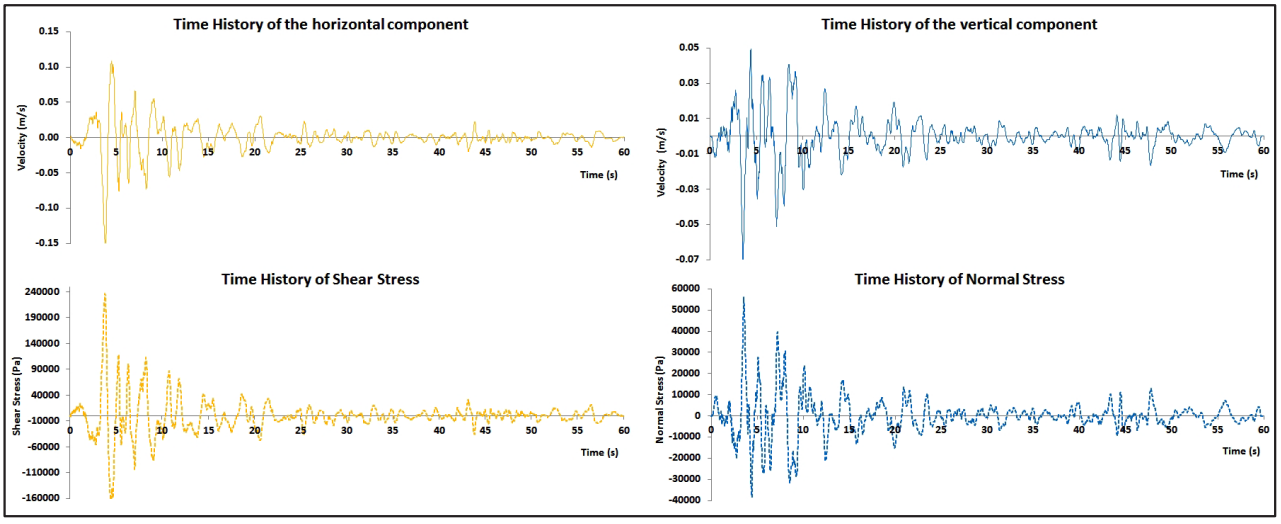

Figure 7: Time histories of the seismic waves input: horizontal ground motion and shear stress (left); vertical ground motion and normal stress (right).

6.2 Dynamic and LSR of the case study analysis

The case study concerns the right trans-tensional fault with a predominantly normal component named 'Candelaro'. The aim is to help shed light on the mechanisms of coseismic rupture, in the case of reactivation of this active and capable normal fault and on the LSR in the projection area of the fault plane onto the ground level. The results of these kinds of simulations have important implications for seismic microzonation of the territory, for the design of new infrastructures and for the safety of existing ones.

The case study dynamic analysis was performed on the geomechanical model as in Fig. 6c, using an input earthquake (dotted blue and yellow lines in Fig. 4), obtained with the software REXEL [38] from the European Strong-motion Database [2], [3]. This earthquake reflects the seismological characteristics of the case study area and is seismocompatible with the 5% damping elastic spectrum of the Italian seismic normative [52].

The maximum displacement obtained, on the order of 0.80–1.30 m (Fig. 9a), occurs deep in the limestone rock mass along the fault hanging wall. Also, it is observed that

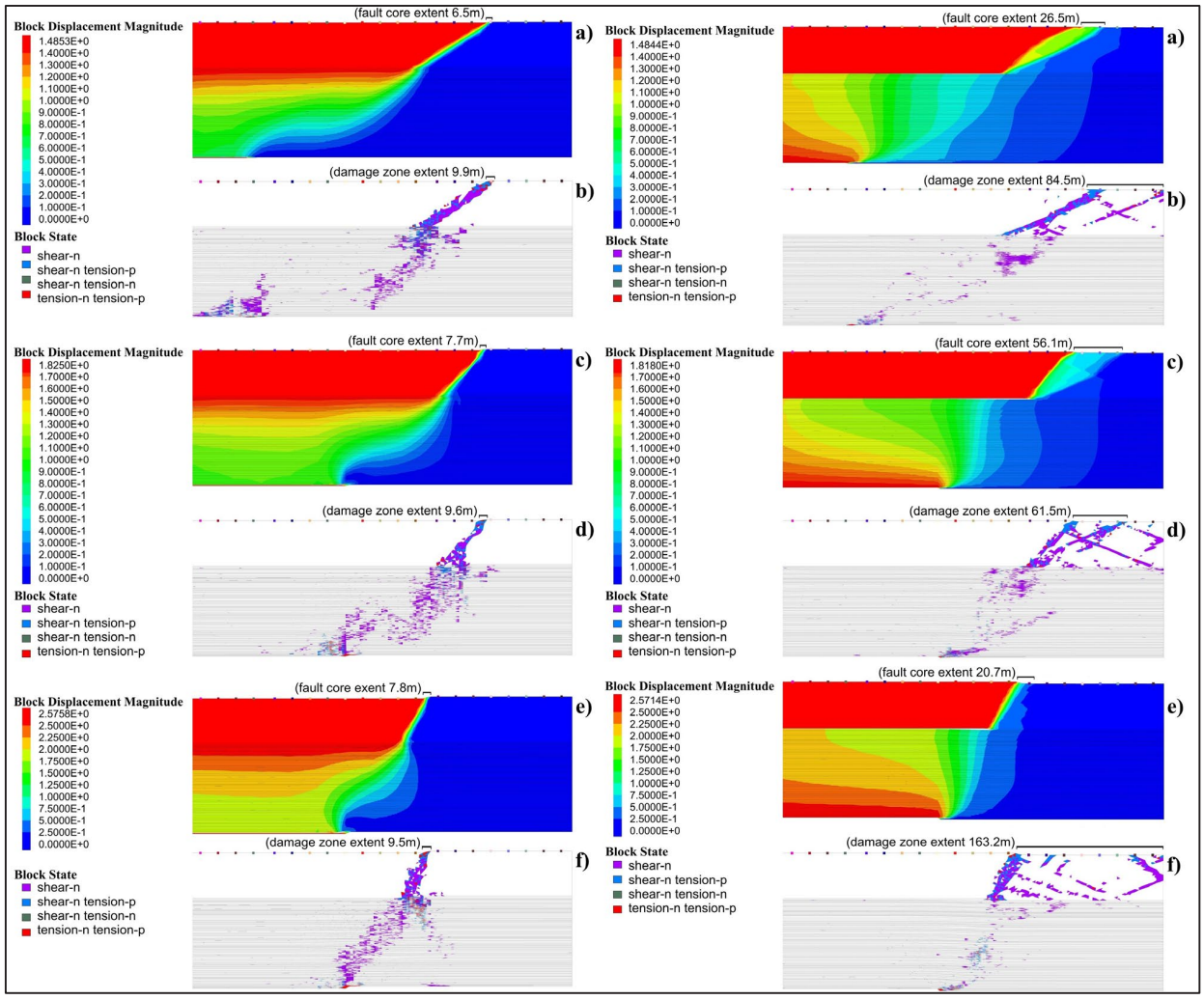

Figure 8: Displacements, fault core and damage zone extents and plastic states in quasi-static analyses of normal fault generation (left) and reverse fault (right): a–b (dip angle 30°); c–d (dip angle 45°); e–f (dip angle 60°).

the failures of the rock mass limestone substrate (Fig. 9b) are caused almost exclusively by shear stresses.

A previous study has shown that soil deformations are not symmetrical [65]. The shear fractures in the limestone substrate are concentrated both along the pre-existing fault plane and along a series of roughly parallel planes to the right and left of it. Interestingly, the main fault plane tends to divide into many conjugate planes with a Graben or flower structure as it moves from the limestone substrate to the calcarenitic cover. Another evidence of the different stress-strain state of the cover rock mass is that its upper portion, on the hanging wall side, is uniformly subject to tensile stresses, while on the footwall side is almost exclusively subject to shear stresses.

Table 5 summarises the values achieved in different ways for the displacements along the fault plane and on the ground level.

Numerical modelling has provided displacements at depths along the fault plane that are in good agreement with those obtained both with the Hanks and Kanamori equation (1) and with geostructural measurements performed in situ on similar normal faults in the Murge area of Apulia [42].

Local seismic response (LSR) analysis, in the presence of layer and fault discontinuities, was conducted with the methodologies commonly used in literature studies [18], [32], [45], [54], [56]. In particular, in order to highlight the contribution on the LSR of the reactivation of a pre-existing fault, simulations were conducted in both the absence (Fig. 10 left) and presence (Fig. 10 right) of a fault plane in the model.

The amplification/deamplification factor (FA) of the X and Y acceleration components of the ground-level motion was analysed to estimate the effects of LSR. More

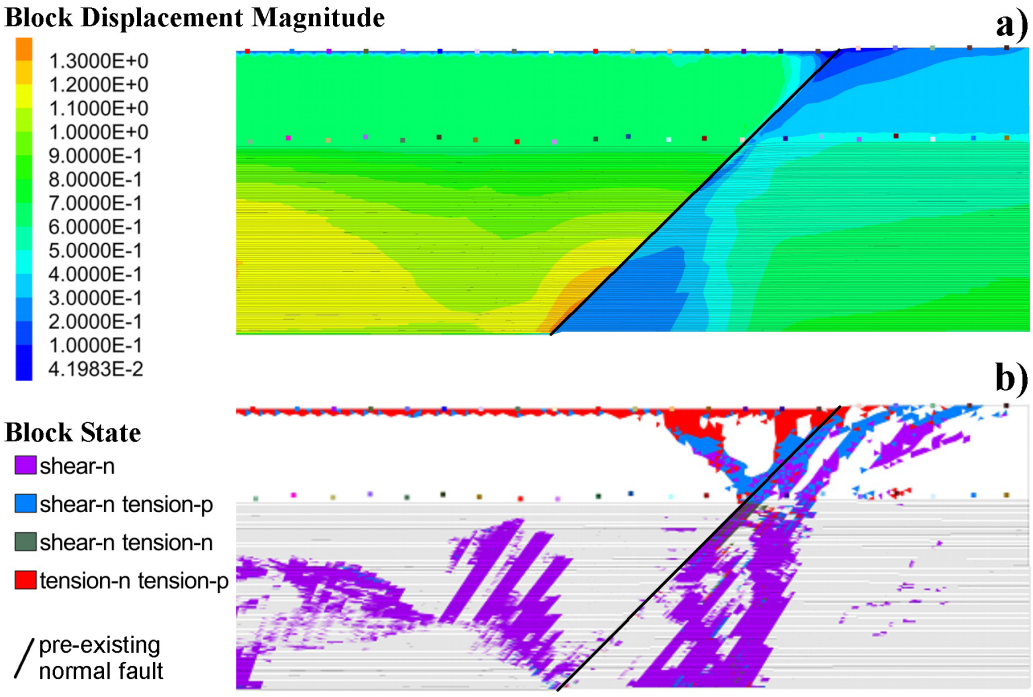

Figure 9: Dynamic case study analysis of the 'Candelaro' active and capable normal fault: a) displacements; b) plastic states.

Table 5: Dynamic case study analysis of the 'Candelaro' active and capable normal fault: failure type, displacement values, extents of fault core and damage zone.

Kinematism	Dip angles (degrees)	Type of failure	Displacement in depth along the fault plane UDEC simulation (m)	Displacement on the ground level UDEC simulation (m)	Displacement on the ground level equation [2] (m)	Displacement along the fault plane - Hanks and Kanamori's equation (m)
Normal fault	45	Conjugate surfaces 'Graben o flower structure'	0.80–1.30	0.1–0.2	0.12	0.92

specifically, in each control point on the ground level of the model (Fig. 6 b, c), the FA has been calculated as a ratio of the values of the X and Y acceleration spectrum in the points at the top of the model and in the corresponding ones at the base of the calcarenitic rock mass for three ranges of vibration periods 0.1–0.5, 0.4–0.8 and 0.7–1.1s. These ranges of vibration periods, normally used in the LSR studies, are also comparable with the natural ones of the most common buildings existing in the case study area.

The LSR trend comparison of the two analysed models allows us to make some considerations about the amplification/deamplification effects at the ground level in an area without a pre-exiting fault (Fig. 10 left) or affected by the reactivation of a capable fault (Fig. 10 right). As can be seen, the LSR of the two models is very different depending on the absence or presence of a pre-existing fault.

In the model without a pre-existing fault, there is a substantial deamplification at the ground surface for all three analysed frequency ranges and for both X and Y motion components (Fig. 10 a, b left). Such deamplification, as already pointed out in previous studies [6], [7], [18], [54], would be explained by the strong dissipation of energy during the plastic deformation of interlayers in the limestone substrate. The model with the pre-existing fault, on the other hand, presents seismic amplification phenomena, for both components of X and

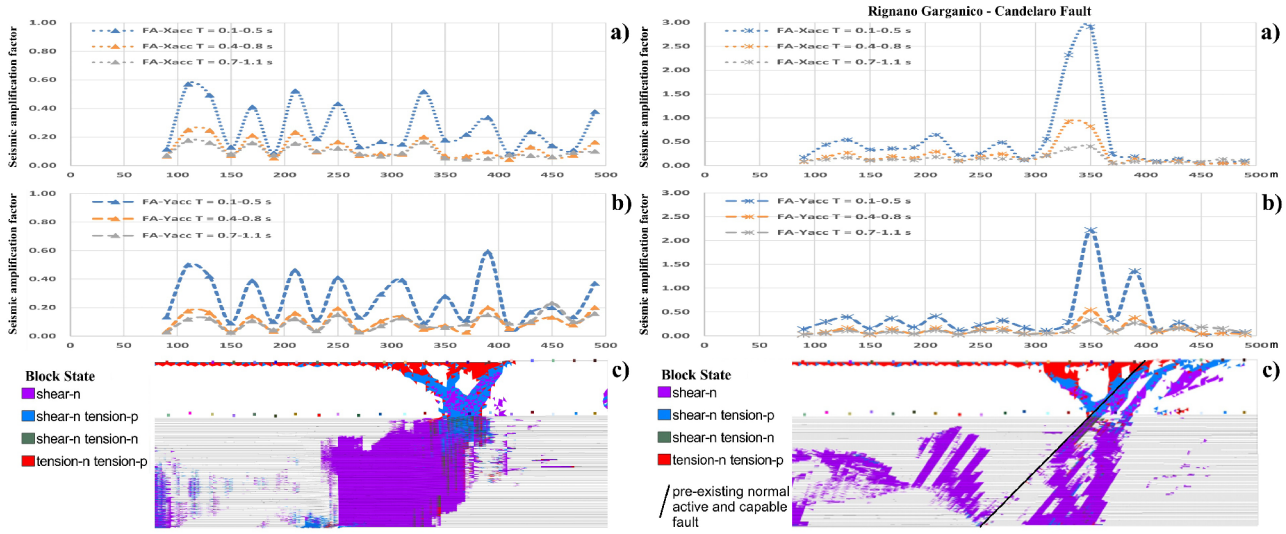

Figure 10: Local seismic response (LSR) of the case study: on the left model without a pre-existing fault plane – a) FA in X-acceleration, b) FA in Y-acceleration, c) plastic states; on the right model of the 'Candelaro' active and capable normal fault plane – a) FA in X-acceleration, b) FA in Y-acceleration, c) plastic states.

Y motion (Fig. 10 a, b right), in the range of vibration periods 0.1–0.5 s and deamplification for the other periods considered. In detail, FA presents a substantially unimodal distribution for X-accelerations and bimodal for Y-accelerations with peak values of FA-Xacc = 2.91, FA-Yacc = 2.22 and FA-Yacc = 1.36, respectively. There seems to be a close correlation between the location of the peak amplification of seismic motion at the surface, in the low period range, the geometry and type of plasticisation zones in the calcarenitic cover with the pre-existing fault. As a matter of fact, the hanging wall zone, which extends about 100 m to the left of the fault plane, has large areas of tensile and shear plasticisation, and it is subject to seismic amplification having the highest FA peaks of both X and Y acceleration components. This particular occurrence could perhaps be explained by the formation of a graben structure, bounded by the fault plane (right) and the plasticisation and shear rupture planes (left). Such discontinuities would result in a kind of constructive entrapment in the reflected/refracted surface seismic waves.

Finally, further confirmation of the accuracy of the physical–mechanical parameters and constitutive models chosen for the dynamic analyses arises from the comparison of the result obtained, in terms of the maximum expected displacement at the ground level, with the numerical simulation (Table 5) and the one calculated using the relationship (2) proposed by the Italian seismic regulations [52]:

$$d_g = 0.025 * a_g * g * FA * T_C * T_D \quad (2)$$

where: a_g = 0.205755g (horizontal acceleration for T = 0 s, see Fig. 6); g = 9.81 m/s² (gravity acceleration); FA = 2.91 (amplification factor of X-accelerations, see Fig. 10 a, on right); T_C = 0.333439s (period of the start of the constant acceleration section, see Fig. 6); T_D = 2.42302s (period of the end of the constant acceleration section, see Fig. 6).

Hence, considering FA = 2.91 obtained from the LSR for the X-accelerations of the ground motion, equation (2) gives a maximum displacement value on the ground level equal to d_g = 0.12 m which is in good agreement with the displacement on the ground level obtained by numerical UDEC simulation (Fig. 9 a and Table 5).

7 Conclusions

Numerical modelling and simulations, conducted on a stratigraphic succession typical of the Apulian territory, have provided results that allow some interesting conclusions to be drawn in agreement with the results of previous studies. This series of parametric analyses is applicable to general cases, concerning the propagation of the first fault under dry conditions, from a stratified limestone substrate to the overlying massive calcarenitic cover. The case study simulation, on the other hand, concerns the coseismic rupture mechanisms in the case of seismic reactivation of an active and capable normal

fault and the local seismic response (LSR) around the fault plane at the ground level.

The following are main conclusions obtained:

parametric analyses with pseudo-static loading

- The fault rupture propagation from the bedrock up to the ground level through the cover rock may deviate significantly from the straight projection of the bedrock fault plane. This phenomenon is most evident in cases of reverse faults, where the damage zone in the calcarenitic cover tends to be more extensive and has a lower dip than the fault plane in the substrate.
- In the cases of reverse faults that dip at 30° and 45°, trailing imbricate fan type shear structures are generated, where the maximum displacement occurs in the shear plane separating the hanging wall from the foot wall (Fig. 8 b, d, on right). Subordinately, there are also conjugate rupture plans. In the case of a reverse fault that dips at 60° (Fig. 8 f), several conjugate rupture planes are generated in addition to the main rupture plane, affecting the fault foot wall of the calcarenitic rock mass.
- Regarding the failure mechanisms of the limestone substrate rock mass and calcarenitic cover, it is observed that they are mainly caused by shear and, subordinately, tensile stress.
- The zone of high brittle fracturing (damage zone) and the probably connected increased permeability tend to be concentrated on the hanging wall, in cases of direct fault models, and in the foot wall, in cases of reverse faults. Moreover, its extent is about 6–16 times smaller in normal faults than in reverse faults.

seismic reactivation of an active and capable normal fault and local seismic response (LSR)

- The main fault plane tends to divide into many conjugate planes, with Graben or flower structure as it moves from the limestone substrate to the calcarenitic cover (Fig. 9 b).
- The stress state of the most superficial portion of the calcarenitic cover is not symmetrical. In fact, on the hanging wall side, it is uniformly subject to tensile stress; on the footwall side, it is subject to shear stress.
- Comparing the results of normal fault dips at 45° for simulations of the quasi-static analyses (Fig. 8 d left) and those of the dynamic analyses (Fig. 9 b), it can be seen that in the former case (conditions of the first rupture of the calcarenitic cover, by fault propagation from the limestone substrate), the fracturing is concentrated almost exclusively along a single plane, which is that of the upward extension of the fault plane.
- The LSR of the model without a pre-existing fault shows a substantial deamplification at the ground surface for all three analysed frequency ranges and for both Xacc and Yacc motion components (Fig. 10 a, b left). Such deamplification would be explained by the strong dissipation of energy during interlayer plastic deformation in the limestone substrate.
- The LSR of the model with a pre-existing fault (case study of 'Candelaro' fault) shows peaks of ground motion amplification, for both FA-Xacc and FA-Yacc components, exclusively in the range of 0.1- to 0.5-s vibration periods (Fig. 10 a, b right).
- FA presents a substantially unimodal distribution for X-accelerations and bimodal for Y-accelerations with peak values of FA-Xacc = 2.91, FA-Yacc = 2.22 and FA-Yacc = 1.36, respectively
- In the LSR of the case study (model with a pre-existing normal fault), there appears to be a close correlation between the position of the peak amplification and the geometry and type of plasticisation zones in the calcarenitic cover. This could be explained by the presence of a Graben structure, bounded by the fault plane (right) and the planes of plasticisation and shear rupture (left), within which a kind of constructive trapping of reflected/refracted surface seismic waves would occur.
- Confirmation of the accuracy of the physical–mechanical parameters and constitutive models chosen for the dynamic numerical analyses of the case study comes from the good agreement among the displacements predicted at the ground level with the numerical simulation, those measured in situ as a result of coseismic ruptures in the 1948 earthquake and those calculated using equations (1) and (2) widely used in the literature and in the Italian building code (NTC18).

Credit authorship contribution statement

Giovanni Bruno: conceptualisation, methodology, numerical analyses, writing original draft. Laura Guerra: methodology, seismic characterisation, selection of the seismic input.

Declaration of Competing Interests

The authors declare that there are no conflicts of interest with this publication.

Data availability

Data will be made available on request.

Funding

This research did not receive any specific grant from funding agencies in the public, commercial or not-for-profit sectors.

References

[1] Abe, S., Gent, H.V., Urai J.L. (2011): DEM simulation of normal faults in cohesive materials. Tectonophysics 512: 12-21.

[2] Ambraseys, N.N., Smit, P., Sigbjornsson, R., Suhadolc, P. and Margaris, B. (2002): Internet-Site for European Strong-Motion Data. European Commission, Research-Directorate General, Environment and Climate Programme.

[3] Ambraseys, N.N., Douglas, J., Rinaldis, D., Berge-Thierry, C., Suhadolc, P., Costa, G., Sigbjornsson, R., Smit, P. (2004): Dissemination of European strong-motion data. Vol. 2, CD-ROM Collection, Engineering and Physical Sciences Research Council, UK.

[4] Anastasopoulos, I., Gazetas, G., Bransby, M.F., Davies, M.C.R., Nahas, E.I. (2007): Fault rupture propagation through sand: finite-element analysis and validation through centrifuge experiments. J. Geotech. Geoenviron. Eng. 133 (8): 943-958.

[5] Baldassarre, G. (1990): Zonazione geologico tecnica della città di Matera. Geol. Appl. e Idrog. vol. XXV: 181-194.

[6] Barbero, M., Barla, G., Demarie, G.V. (2004): Applicazione del Metodo degli Elementi Distinti alla dinamica di mezzi discontinui. Rivista Italiana di Geotecnica 3.

[7] Barla, G., Monacis, G., Perino, A., Hatzor, Y.H. (2010): Distinct Element Modelling in Static and Dynamic Conditions with Application to an Underground Archaeological Site. Rock Mechanics and Rock Engineering 43 (6): 877-890.

[8] Bense, V.F., Gleeson, T., Loveless, S.E., Bour, O., Scibek, J. (2013): Fault zone hydrogeology. Earth-Science Reviews 127: 171-192.

[9] Billi, A. (2005): Attributes and influence on fluid flow of fractures in foreland carbonates of southern Italy. J. Struct. Geol. 27: 1630-1643.

[10] Billi, A., Salvini, F., Storti, F. (2003): The damage zone-fault core transition in carbonate rocks: Implications for fault growth, structure and permeability. J. Struct. Geol. 25: 1779-1794.

[11] Bransby, M.F., Davies, M.C.R., EL Nahas, A. (2008a): Centrifuge modeling of normal fault-foundation interaction. Bull. Earthq. Eng. 6 (4): 585-605.

[12] Bray, J.D., Seed, R.B., Cluff, L.S., Seed, H.B. (1994a): Earthquake fault rupture propagation through soil. J. Geotech. Eng. 120 (3): 543-561.

[13] Bray, J.D., Seed, R.B., Seed, H.B. (1994b): Analysis of earthquake fault rupture propagation through cohesive soil. J. Geotech. Eng. 120 (3): 562-580.

[14] Bruno, G. (2012): Caratterizzazione geomeccanica per la progettazione ingegneristica. Flaccovio Dario (ed.), Palermo, ISBN 978-88-579-0150-3.

[15] Bruno, G., Cherubini, C. (2005): Subsidence Induced by the Instability of Weak Rock Underground Quarries in Apulia. Giornale di Geologia Applicata 1: 33-39. https://doi.org/10.1474/GGA.2005-01.0-04.0004.

[16] Bruno, G., Tupputi, D., Cristallo, F. (2016): Ricostruzione con metodi geofisici del modello ipogei-struttura della chiesa di San Domenico (Matera) finalizzato a valutazioni di stabilità. Geologia dell'Ambiente, Supplemento al n. 3/2016, ISSN 1591-5352.

[17] Bruno. G., Rotolo, M. (2018): Analisi di stabilità di un frantoio ipogeo ubicato sul fianco di un versante in roccia calcarenitica in agro di Monopoli. Geologi e Territorio 2: 3-8, ISSN 1974-1189.

[18] Bruno, G. and Carucci, F. (2020): 2D numerical analysis of the seismic response of a karst rock mass: importance of underground caves and geostructural details. Studia Geotechnica et Mechanica, vol. 42, no. 1, 2020, 61-73. https://doi.org/10.2478/sgem-2019-0028.

[19] Bruno, G., Tupputi, D., Simeone, V. (2023): Geomechanical modelling and stability analysis of the shallow underground water reservoir 'Palombaro Lungo' (Matera-Italy). Environmental Earth Sciences, (2023) 82:302. https://doi.org/10.1007/s12665-023-11001-2.

[20] Chang, Y.Y., Lee, C.J., Huang, W.C., Hung, W.Y, Huang, W.J., Lin, M.L., Chen, Y.H. (2015): Evolution of the surface deformation profile and subsurface distortion zone during reverse faulting through overburden sand. Engineering Geology 184 (2015): 52-70.

[21] Chen, C.C., Huang, C.T., Cherng, R.H., Jeng, V. (2000): Preliminary investigation of damage to near fault buildings of the 1999 Chi-Chi earthquake. Earthq. Eng. Eng. Seismol. 2 (1), 7: 9-92.

[22] Chen, W.S., Yang, C.C., Yen, I.C., Lee, L.S., Lee, K.J., Yang, H.C., Ota, Y., Lin, C.W., Lin, W.H., Shih, T.S., Lu, S.T. (2007): Late Holocene paleoseismicity of the southern part of the Chelungpu Fault in Central Taiwan: evidence from the Chushan excavation site. Bull. Seismol. Soc. Am. 97 (1B): 1-13.

[23] Cherubini, C., Reina, A., Bruno, D. (2007): Le rocce tenere del Salento: proposta di classificazione con l'uso delle caratteristiche tecniche e meccaniche. Geologi e Territorio 2: 37-47, ISSN 1974-1189.

[24] Chilovi, C., De Feyter, A.J. e Pompucci, A. (2000): Wrench zone reactivation in the Adriatic Block: the example of the Mattinata Fault System (SE Italy). Boll. Soc. Geol. It., 119: 3-8.

[25] Commissione tecnica per la microzonazione sismica (2015): Linee guida per la gestione del territorio in aree interessate da Faglie Attive e Capaci (FAC), versione 1.0. Conferenza

delle Regioni e delle Province Autonome - Dipartimento della protezione civile, Roma.

[26] Cotecchia, V., Grassi, D. (1975): Stato di conservazione dei "sassi" di Matera (Basilicata) in rapporto alle condizioni geomorfologiche e geomeccaniche del territorio e alle azioni antropiche. Geol. Appl. ed Idrog. vol. X: 55-105.

[27] De Santis, V., Caldara, M. & Pennetta, L. (2013): The marine and alluvial terraces of Tavoliere di Puglia plain (southern Italy). Journal of Maps, DOI:10.1080/17445647.2013.861366

[28] DISS Working Group (2021): Database of Individual Seismogenic Sources (DISS), version 3.3. Istituto Nazionale di Geofisica e Vulcanologia (INGV). https://diss.ingv.it/diss330/dissmap.html. Accessed 01 June 2023.

[29] Dong, J.J., Wang, C.D., Lee, C.T., Liao, J.J., Pan, Y.W. (2003): The influence of surface ruptures on building damage in the 1999 Chi-Chi earthquake: a case study in Fengyuan City. Engineering Geology 71, Issues 1-2, January 2004: 157-179.

[30] Faulkner, D.R., Jackson, C.A.L., Lunn, R.J., Schlische, R.W., Shipton, Z.K., Wibberley, C.A.J., Withjack, M.O. (2010): A review of recent developments concerning the structure, mechanics and fluid flow properties of fault zones. Journal of Structural Geology 32: 1557-1575.

[31] Geological Society of London, Engineering Group Working Party (1970) Report on the logging of rock cores for engineering purposes. Q. J. Eng. Geol. 3: 1-24.

[32] Ghosh, A., Hsiungm S. (2011): Effects of tilted and faulted strata on seismic ground motion. U.S. Nuclear Regulatory Commission Contract NRC-02-07-006, Center for Nuclear Waste Regulatory Analyses, San Antonio, Texas.

[33] Guidoboni, E., Ferrari, G., Mariotti, D., Comastri, A., Tarabusi, G., Sgattoni, G., Valensise, G. (2018): CFTI5Med, Catalogo dei Forti Terremoti in Italia (461 a.C.-1997) e nell'area Mediterranea (760 a.C.-1500). Istituto Nazionale di Geofisica e Vulcanologia (INGV). https://doi.org/10.6092/ingv.it-cfti5.

[34] Guidoboni, E., Ferrari, G., Tarabusi, G., Sgattoni, G., Comastri, A., Mariotti, D., Ciuccarelli, C., Bianchi, M.G., Valensise, G. (2019): CFTI5Med, the new release of the catalogue of strong earthquakes in Italy and in the Mediterranean area. Scientific Data 6, Article number: 80 (2019). https://doi.org/10.1038/s41597-019-0091-9. Accessed 01 June 2023.

[35] Hanks, T.C., Kanamori, H. (1979): A moment-magnitude scale. J. Geophys. Res. 84: 2348-2350.

[36] IAEA SSG-9 (2010) Seismic Hazard in Site Evaluation for Nuclear Installations. *Specific Safety Guide. IAEA Safety Standards. Series.* https://www-pub.iaea.org/MTCD/publications/PDF/Pub1448_web.pdf. Accessed 01 June 2023.

[37] IAEA TECDOC 1767 (2015) The Contribution of Palaeoseismology to Seismic Hazard Assessment in Site Evaluation for Nuclear Installations. https://www-pub.iaea.org/MTCD/Publications/PDF/TE-1767_web.pdf. Accessed 01 June 2023.

[38] Iervolino, I., Galasso, C., Cosenza, E. (2010): REXEL: computer aided record selection for code-based seismic structural analysis. in Bulletin of Earthquake Engineering, n.8: 339-362.

[39] ISIDe Working Group (2007): Italian Seismological Instrumental and Parametric Database (ISIDe). Istituto Nazionale di Geofisica e Vulcanologia (INGV). https://doi.org/10.13127/ISIDE. Accessed 01 June 2023.

[40] ITHACA Working Group (2019): ITHACA (ITaly HAzard from CApable faulting), A database of active capable faults of the Italian territory. https://sgi.isprambiente.it/ithaca/viewer/index.html. Accessed 01 June 2023.

[41] Itasca (2019): Universal Distinct Element Code: User's Guide. Itasca Consulting Group, Inc. Minneapolis, Minnesota 55401 USA.

[42] Korneva, I., Tondi, E., Agosta, F., Rustichelli, A., Spina, V., Bitonte, R., Di Cuia, R. (2014): Structural properties of fractured and faulted Cretaceous platform carbonates, Murge Plateau (southern Italy). Marine and Petroleum Geology 57: 312-326.

[43] Lin, M.L., Lu, C.Y., Chang, K.J., Jeng, F.F., Lee, C.J. (2005): Sandbox experiments of plate convergence-scale effect and associated mechanism. Terr. Atmos. Ocean., Sci. 16 (3): 595-620.

[44] Lin, M-L., Chung, C-F., Jeng, F-S. (2006): Deformation of overburden soil induced by thrust fault slip. Engineering Geology 88 (1-2): 70-89.

[45] Loukidis, D., Bouckovalas, G. (2001): Numerical simulation of active fault rupture propagation through dry soil. In: Proceedings of the fourth international conference on recent advances in geotechnical earthquake engineering and soil dynamic, Prakash S. Editor, San Diego, California, CD-ROM, paper no. 3.04.

[46] Loukidis, D., Bouckovalas, G.D., Papadimitriou, A.G. (2009): Analysis of fault rupture propagation through uniform soil cover. Soil Dynamics and Earthquake Engineering 29: 1389-1404.

[47] Micarelli, L., Moretti, I., Jaubert, M., Moulouel, H. (2006): Fracture analysis in the south-western Corinth rift (Greece) and implications on fault hydraulic behavior. Tectonophysics 426: 31-59.

[48] Ministry for the Environment, New Zealand (2003): Planning for the development of land on or close to active faults. A guideline to assist resource management planners in New Zealand, ISBN: 0-478-18901 ME number: 483.

[49] Mortazavi Zanjani, M., Soroush, A. (2013): Numerical modeling of reverse fault rupture propagation through clayey embankment. Int. J. Civ. Eng. 11 (2): 122-132.

[50] Ng, C.W.W., Cai, Q.P., Hu, P. (2012): Centrifuge and numerical modeling of normal fault rupture propagation in clay with and without a preexisting fracture. J. Geotech. Geoenviron. Eng. ASCE, 138 (12): 1492-1502.

[51] Nollet, S., Kleine Vennekate, G.J., Giesew, S., Vrolijk, P., Urai, J.L., Ziegler, M. (2012): Localization patterns in sandbox-scale numerical experiments above a normal fault in basement. J. Struct. Geol. 39: 199-209.

[52] NTC18 Norme Tecniche per le Costruzioni (2018): Ministero Infrastrutture e Trasporti, DM 17 Gennaio 2018, Gazzetta Ufficiale della Repubblica Italiana 42, 2018.

[53] Papadimitriou, A., Loukidis, D., Bouckovalas, G., Karamitros, D. (2007): Zone of excessive ground surface distortion due to dip-slip fault rupture. 4th International Conference on Earthquake Geotechnical Engineering, June 25-28, 2007, Paper No. 1583.

[54] Pyrak-Nolte, L.J., Myer, L.R., Cook Neville, G.W. (1990): Transmission of Seismic Waves Across Single Natural Fractures. Journal of Geophysical Research, vol. 95, n° B6, June 10: 8617-8638.

[55] Ranieri, L. (1949): Sul periodo sismico dell'estate 1948 in Puglia. Bollettino della Società Geografica Italiana, a. 83, vol.86: 273-219, Roma.

[56] Rodriguez-Castellanos, A., Sánchez-Sesma, F.J., Luzón, F. and Martin, R. (2006): Multiple scattering of elastic waves by subsurface fractures and cavities. in Bulletin of the Seismological Society of America, vol. 96, n. 4A: 1359-1374.
[57] Roth, W.H., Kalsi, G., Papastamatiou, D., Cundall, P.A. (1982): Numerical modelling of fault propagation in soils. In: Proceedings of the fourth international conference on numerical methods in geomechanics, Edmonton, Canada, pp. 487-494.
[58] Servizio Geologico d'Italia (2011): Note Illustrative della Carta Geologica d'Italia alla scala 1:50000 Foglio 396 San Severo. Istituto Superiore per la Protezione e la Ricerca Ambientale (ISPRA), Roma.
[59] Simeone, V., Doglioni, A., Lacertosa, R.M., Sdao, F. (2019): Environmental and Geological Characters and Stability Problems in the Historic Centre of Matera (South Italy). In: Shakoor A and Cato K (eds.) IAEG/AEG Annual Meeting Proceedings, ISBN 978-3-319-93127-2 (eBook); San Francisco, California, 2018, Volume 2, pp. 161-168. https://doi.org/10.1007/978-3-319-93127-2_23.
[60] Spalluto, L. (2004): La Piattaforma Apula nel Gargano centro-occidentale: organizzazione stratigrafica ed assetto della successione mesozoica di piattaforma interna. Tesi di dottorato in Scienze della Terra, Università degli Studi di Bari, 173 pp.
[61] Spalluto, L. and Moretti, M. (2006): Evidenze di neotettonica (Pliocene medio-Pleistocene superiore) nel settore occidentale del promontorio del Gargano (Italia meridionale). Il Quaternario, Italian Journal of Quaternary Sciences 19 (1): 143-154.
[62] Taniyama, H. (2011): Numerical analysis of overburden soil subjected to strike-slip fault: distinct element analysis of Nojima fault. Eng. Geol. 123 (3): 194-303.
[63] Vitale, S., Amore, O.F., Ciarcia, S., Fedele, L., Grifa, C., Prinzi, E.P., Tavani, S., Assisi Tamparulo, F. (2017): Structural, petrographic, and petrological clues for a Cretaceous-Paleogene abortive rift in the southern Adria domain (southern Apennines, Italy). Geol. J.. https://doi.org/10.1002/gj.2919.
[64] Well, D.L. and Coppersmith, K.J. (1994): New Empirical Relationships among Magnitude, Rupture length, rupture width, rupture area and surface displacement. Bulletin of the Seismological Society of America, vol. 84, No. 4: 914-1002.
[65] Wesnousky, S.G. (2008): Displacement and geometrical characteristics of earthquake surface ruptures, Bull. Seismol. Soc. Am. 98: 1609-1632.